JAERI-M
9358

MAGNET DESIGN FOR JAERI HEAVY-ION SPECTROGRAPH

February 1981

Yasuharu SUGIYAMA, Naomoto SHIKAZONO
Takemi SATO*, Takeshi TAKAYAMA* and
Hidetsugu IKEGAMI**

日本原子力研究所
Japan Atomic Energy Research Institute

JAERI-M 9358

Magnet Design for JAERI Heavy-Ion Spectrograph

Yasuharu SUGIYAMA, Naomoto SHIKAZONO, Takemi SATO*
Takeshi TAKAYAMA* and Hidetsugu IKEGAMI**
Division of Physics, Tokai Research Establishment, JAERI

(Received January 31, 1981)

The magnet design has been carried out for two dipoles (D1,D2), one quadrupole (Q) and three multipoles (M1,M2,M3) of which the JAERI heavy-ion spectrograph consists. The poles and yokes of all magnets are made of the highly pure forged irons with a carbon content of less than 0.02 % or the fully killed and rolled irons with a carbon content of less than 0.04 %. Cares are paid to avoid the magnetic saturation in the irons. All corners of the pole edges of the dipole magnets are shaped in Rogowski's curve which is approximated by the successions of steps. Current sheet magnets are adopted for the construction of the multipole magnets. Coil configurations of the multipole magnets are determined after the extensive numerical calculations of the field distributions.

Keywords : JAERI Heavy-Ion Spectrograph, Magnet Design, Dipole Magnets, Quadrupole Magnet, Multipole Magnets

---

* Sumitomo Heavy Industries,LTD
** Research Center for Nuclear Physics, Osaka University, Suita, Osaka, Japan

JAERI-M 9358

原研重イオンスペクトログラフ用電磁石の設計

日本原子力研究所東海研究所物理部
杉山康治・鹿園直基・佐藤岳実＊・高山　猛＊
池上栄胤＊＊

（１９８１年１月３１日受理）

原研重イオンスペクトログラフを構成する２つの２極電磁石（Ｄ１，Ｄ２），１つの４極電磁石（Ｑ），３つの多極電磁石（Ｍ１，Ｍ２，Ｍ３）の設計を行った。すべての電磁石のポールとヨークは炭素含有量が0.０２％以下の鍛造された純鉄か，炭素含有量が0.０４％以下の圧延された鉄から作られ，その鉄中で磁場の飽和が生じないよう注意が払われている。２極電磁石のポールのすべての境界は階段状に近似したロゴスキー曲線で形成した。また多極電磁石にはカレントシート型電磁石を採用した。多極電磁石のコイル形状は磁場分布の広範囲にわたる数値計算の結果決定した。

＊　住友重機械工業株式会社
＊＊ 大阪大学核物理研究センター

Contents

目　　次

1. Introduction

The JAERI heavy-ion magnetic spectrograph has been designed in order to fully explore a rich variety of phenomena expected from heavy ion collisions with the JAERI 20 MV tandem accelerator.[1] The spectrograph consists of the quadrupole (Q), the multipole (M1), the dipole (D1), the multipole (M2), the dipole (D2) and the multipole (M3). The geometrical arrangement of the spectrograph is shown in fig. 1. Characteristic features of the spectrograph are as follows.

1) In order to obtain unique mass identification over a wide mass range in combination with time-of-flight measurement, a path length difference ΔL is kept small: $L/\Delta L$ is larger than 210 for a horizontal angular spread of 5 mrad.
2) A momentum resolving power $p/\Delta p$ of 7400, which is suitable for high resolution works with heavy ions, is obtainable for solid angle up to 16 msr.
3) A wide range of kinematic correction from k=-0.4 to 1.0 is possible by the use of the M2 magnet.
4) The dispersion is variable from D=10 to 15.5 cm/% along the focal plane for k=0 by the use of the M3 magnet.

The calculated ion-optical specifications are summarized in table 1.

The ion-optical performance greatly depends on actual field distributions in the magnets of the spectrograph. In order to realize the calculated ion-optical specifications, extensive design studies for each magnet has been carried out. In this study many experiences with the spectrograph RAIDEN of

Osaka university[2] are introduced on the practical construction. Especially the current sheet magnets developped by Ikegami et al [3] are adopted for the construction of the multipole magnets M1, M2 and M3. In the following sections design works are described for each magnet.

2. Magnet design

The required specifications of each magnet are tabulated in table 2.

2.1 Dipole magnets D1 and D2

In order to achieve a high uniformity in the magnetic field over a full range of the field strength, irons with high permeability should be used for poles and yokes. The field non-uniformity caused by the return path difference of the flux is reduced by the use of such irons. The material of the poles chosen are the highly pure forged iron with a carbon content of less than 0.02 %. The yokes are made of the fully killed and rolled iron with a carbon content of less than 0.04 %.

As is shown in table 2 narrow tolerance is set in machining and positioning the poles, since errors in the optical geometry seriously deteriorate the performance of the spectrograph.

Deflection of poles and yokes due to magnetic forces is one of the important sources of the field non-uniformity. At full power the yoke structure is estimated to have central deflection of about 0.05 mm. In order to keep the pole

Osaka university[2] are introduced on the practical construction. Especially the current sheet magnets developped by Ikegami et al [3] are adopted for the construction of the multipole magnets M1, M2 and M3. In the following sections design works are described for each magnet.

2. Magnet design

The required specifications of each magnet are tabulated in table 2.

2.1 Dipole magnets D1 and D2

In order to achieve a high uniformity in the magnetic field over a full range of the field strength, irons with high permeability should be used for poles and yokes. The field non-uniformity caused by the return path difference of the flux is reduced by the use of such irons. The material of the poles chosen are the highly pure forged iron with a carbon content of less than 0.02 %. The yokes are made of the fully killed and rolled iron with a carbon content of less than 0.04 %.

As is shown in table 2 narrow tolerance is set in machining and positioning the poles, since errors in the optical geometry seriously deteriorate the performance of the spectrograph.

Deflection of poles and yokes due to magnetic forces is one of the important sources of the field non-uniformity. At full power the yoke structure is estimated to have central deflection of about 0.05 mm. In order to keep the pole

gap free from such a deflection, small gap of 1 mm is prepared between the pole and the yoke. The thicknesses of the poles are chosen to be 210 mm and 200 mm for the D1 and D2 magnets, respectively, so that errors of greater than 0.02 mm may not be caused in the pole gaps by the atmospheric pressure and attractive forces between the magnetized poles.

In general the region of the uniform field is reduced at high fields because of a local magnetic saturation in irons at the corners of the pole edges. The extent of the reduction greatly depends on the shape of the corner. The effect of the shape of the corner on the field distribution has been searched with the program TRIM.[4] At the maximum field strength of 15.5 k gauss the field distributions have been calculated for different shapes of corners. The results are shown in fig.2. As is shown in the figure, the corners are shaped in slanting straight lines. The relative ampere-turns needed to excite the maximum field are also shown in the figure. It is seen that the uniform field regions become wider and the ampere-turns become less as the areas of the slanting straight line become larger. This reflects that the shapes of the corners become closer to the magneto-static equi-potential contour which reduces the local saturation. At the regions of the side boundaries of the pole the required uniform field is possible to be produced by the shape of the corner labeled as No.4 in fig.2. However, this simple shape of the slanting straight line makes the field distribution slightly dependent on the field strength. The small change of the field distribution on the way of the particles gives

a large effect on the focus condition. In order to keep the field distribution independent of the field strength , the shape of Rogowski's curve is desirable. Therefore the corners of the pole edges at the entrance and exit boundaries have been determined to be shaped in Rogowski's curve. For reasons of machining , the corners at the side boundaries are also shaped in Rogowski's curve. The Rogowski's curve is approximated by the successions of the steps for the ease of machining as is shown in fig.3.

Field clamps are prepared at the outsides of the entrance and exit boundaries of the poles to terminate the fringing field distributions and are grounded magnetically to the yokes. The positions of the field clamps have been determined so as to generate the required effective field boundaries. Cares have been paid to avoid a magnetic saturation in the field clamps. The adopted position of the field clamp, the effective field boundary and the fringing field distribution for the D2 magnet are also shown in fig.3. The cross-sectional views of the D1 and D2 magnets are presented in figs.4 and 5, respectively.

2.2 Quadrupole magnet Q

The field strength and the aperture of the quadrupole magnet Q required from the ion-optical calculation are similar to those of the quadrupole magnet used in the spectrograph RAIDEN[2]. Therefore the structure of the quadrupole magnet used in RAIDEN has been introduced in the magnet design. Some modifications of the pole contour have been made in order

to produce a wide uniform region of a field gradient over a full range of the field strength. In fig.6 the structure of the Q magnet is shown . In fig.7 the distributions of the field gradients k calculated with the program LINDA[5] are shown for various field strength along the x-axis at the middle of the magnet. It is seen in fig.7 that the uniformity of the field gradient of less than 10^{-3} is obtainable up to the field gradient of 1.3 kG/cm for the full beam aperture.

2.3 Multipole magnets

Current sheet multipole magnets developped by Ikegami et al. are successfully used in RAIDEN[2]. One of the advantages of the current sheet multipole magnet is that several multipole field components are produced with a high degree of the desired precision in a single magnet. This leads to the reduction of the magnetic space in which the multipole components must be generated. In the present case several multipole field components are required to be generated in the M1, M2 and M3 magnets and the spaces available for these magnets are limited. Therefore current sheet magnets are adopted for the M2 and M3 magnets. Because of the spatial limitation, the special shape of the poles is chosen to produce multipole fields for the M1 magnet.

2.3.1 M1 magnet

The function of the M1 magnet is to cancel the aberrations due to the vertical beam spreads. This magnet is located at the entrance of the D1 magnet. The space for the insta-

llation is so small that the M1 magnet has to be inserted between the upper and the lower coils of the D1 magnet. Then the structure shown in fig.8 has been adopted. This type of the multipole magnet is used in RAIDEN and sextupole field is produced. In the present case the octupole field is needed to be produced as well as the sextupole field in the M1 magnet. The ratio of the field strengths of the sextupole and octupole components is allowed to be constant, following the ion-optical consideration.

In order to determine the structure of the M1 magnet, equi-potential contours of the magneto-static potential are calculated. The magneto-static potential for the 2N-pole field can be written as

$$\phi_{2N} = -\frac{1}{N} k_{2N} r^N \sin(N\theta), \qquad (1)$$

where r and θ are expressed as $r=(x^2+y^2)^{1/2}$ and $\theta=\tan^{-1}(y/x)$, respectively and the axes of x and y are shown in fig.8. The coefficient k_{2N} represents the field strength of the 2N-pole. In the present calculation k_6=40 G/cm^2 and k_8=1.28 G/cm^3 are taken. The required magneto-static potential of the M1 magnet is written as

$$\phi(M1) = \phi_6 + \phi_8 = -13.33\, r^3 \sin(3\theta) - 0.32\, r^4 \sin(4\theta). \qquad (2)$$

In fig.9 several equi-potential contours calculated from eq. (2) are shown by dotted lines. The equi-potential contours which meet the magnet apperture required from the

ion-optical calculation are chosen as the pole contours of the M1 magnet and approximated by circular curves. The pole configurations shown by solid lines in fig.9 have been adopted after some try-and-error works including numerical calculations of field distributions for various geometries. The ideal magnetic field distribution of 2N-pole is expressed in the midplane as

$$B_y^N(y=0)=k_{2N}\, x^{N-1} \quad . \tag{3}$$

The calculated field distribution based on the geometry in fig.9 is compared with the ideal field of eq.(3) and difference ΔB is plotted along x-axis in fig.10. It is clealy seen that the M1 magnet can produce well the required field.

2.3.2 M2 and M3 magnets

The apertures of the M2 and M3 magnets have large horizontal width and relatively small hights. The structure for these magnets is shown schematically in fig.11. Following the formula of the current sheet magnet[3], the current distribution j_{2N} along the inside of the yoke needed to produce the 2N-pole field in the magnet is written as

$$j_{2N}=k_{2N}\, r^{N-1} \sin\{\alpha+(N-1)\theta\} \, , \tag{4}$$

where α represents the inclination of the yoke to the x-axis. The current distribution is realized by wounding coils around

the yoke.

The M2 magnet located between the D1 and D2 magnets provides the kinematic compensation. Following the ion-optical considerations, the multipole components of up to decapole have been required. Among these multipole components, the quadrupole component is the most important for the kinematic compensation. The relatively strong field of up to 180 G/cm has been required. Therefore copper hollow conductors of the outer dimensions 6x12 mm^2 have been chosen for the coils of the quadrupole component. For the other components the coils are made of copper conductors of the dimensions 2x13.58 mm^2 for the sextupole and 1.6x13.58 mm^2 for the octupole and decapole. The configuration of the coil for each component is determined basically from eq.(4). According to the finite dimensions of the conductors, the theoretical current distribution of eq.(4) is only approximately obtainable. In order to obtain the required field distributions by such approximated current distributions, various configurations of the coils were searched with the program TRIM. The calculated field distribution based on the obtained configuration of the coils is compared with the ideal one of eq.(3) for each multipole component and difference B is plotted along the x-axis in the midplane in fig.12. It is clear that the required field distributions are obtainable with a high degree of the precision. In order to avoid the magnetic saturation in the yoke at high fields, the yoke is made of the fully killed and rolled iron with a carbon content of

less than 0.04 % whose width is 200 mm.

The M3 magnet is used for changing the dispersion and located behind the D2 magnet. The required field components are the quadrupole and sextupole. The coil material is chosen to be copper conductors of the dimensions 2x13.58 mm^2. The coil configurations are determined through the same procedure as the case of the M2 magnet. The deviations of the calculated field distribution of each component from the ideal one are shown along the x-axis in fig.13. The precise field distribution is obtainable in the M3 magnet as well as in the M2 magnet.

References

1) Y. Sugiyama, N.Shikazono, H.Ikezoe and H.Ikegami, Contribution to the International Conference on Charged Particle Optics, Giessen, West Germany, Sep. 1980

2) H.Ikegami, S.Morinobu, I.Katayama, M.Fujiwara and S.Yamabe, Nucl. Instr. and Meth. 175 (1980) 335

3) H.Ikegami, Sixth International Conference on Magnet Technology (MT-6), Bratislava (1977) 904; H.Ikegami, T.Takayama, M.Fujiwara, I.Katayama and S.Morinobu,ibid 908; H.Ikegami, T.Takayama, M.Fujiwara, I.Katayama and S.Morinobu, Annual Report 1976, RCNP Osaka University, p 137; H.Ikegami, to be published in Nucl. Instr. and Meth.

4) A.M.Winslow, UCRL 7784-T, Rev.2 (1964); J. Comp. Phys. 1 (1966) 149

5) J.S.Colonias, Particle Accelerator Design; Computer Program (Academic Press) 1974, p 39

Table 1 Calculated ion-optical specifications

Median orbit radius	110 cm
Deflection angle	80° for D1 72° for D2
Angular range	-150° to 85°
Focal line length	130 cm, straight
Tilt angle of focal line	45°
Maximum particle rigidity	17 kG·m
Magnification · horizontal[a)]	2.1
Magnification · vertical	1.7
Variable momentum dispersion[a)]	10.0 to 15.6 cm/%
Momentum range	10 %
Momentum resolving power[b)]	7400
Flight path length	780 cm
Mass resolving power[c)]	210
Acceptance angle · horizontal	± 60 mrad
Acceptance angle · vertical	± 70 mrad
Solid angle	16 msr
Kinematic correction k	-0.4 to 1.0

a) Values are given along the focal line.

b) The particle source width is assumed as 1.0 mm.

c) Horizontal angular spread is assumed as $2\theta_0$=5 mrad.

Table 2 Specifications of the magnets in the spectrograph

Dipole magnets

	D1	D2
Magnet gap	80 mm	100 mm
Pole width	850 mm	1400 mm
Deflection angle	80°	72°
Ampere turn	65230 AT/coil	77274 AT/coil
Maximum magnetic field	15.5 kG	15.5 kG
Thickness of the poles	210 mm	200 mm
Flatness of the pole face	< 0.05 mm	< 0.05 mm
Regularity of the magnet gap	< 0.05 mm	< 0.05 mm
Identity of the pole contour	< 0.1 mm	< 0.1 mm
Position tolerance betwee the poles in the horizontal direction	< 0.2 mm	< 0.2 mm
Total maximum power in coils	107 kW	146 kW

Quadrupole magnet

Magnet aperture	140 mm in diam.
Ampere turn	34531 AT/coil
Maximum field gradient	1.5 kG/cm
Magnet length	220 mm
Identity of the pole contour	< 0.1 mm
Regularity of the pole grouping	< 0.1 mm
Total maximum power in coils	25 kW

Multipole magnets

Magnet	Multipoe	Aperture	Geometrical length	Maximum field strength	Maximum power in coils
M1	sextupole	234mm×100mm	160 mm	25 G/cm^2	16 kW
	octupole			0.8 G/cm^3	
M2	quadrupole	640mm×100mm	400 mm	180 G/cm	157 kW
	sextupole			1.3 G/cm^2	17 kW
	octupole			0.014 G/cm^3	6.3 kW
	decapole			0.00048 G/cm^4	8.0 kW
M3	quadrupole	860mm×100mm	350 mm	75 G/cm	17 kW
	sextupole			0.75 G/cm^2	8 kW

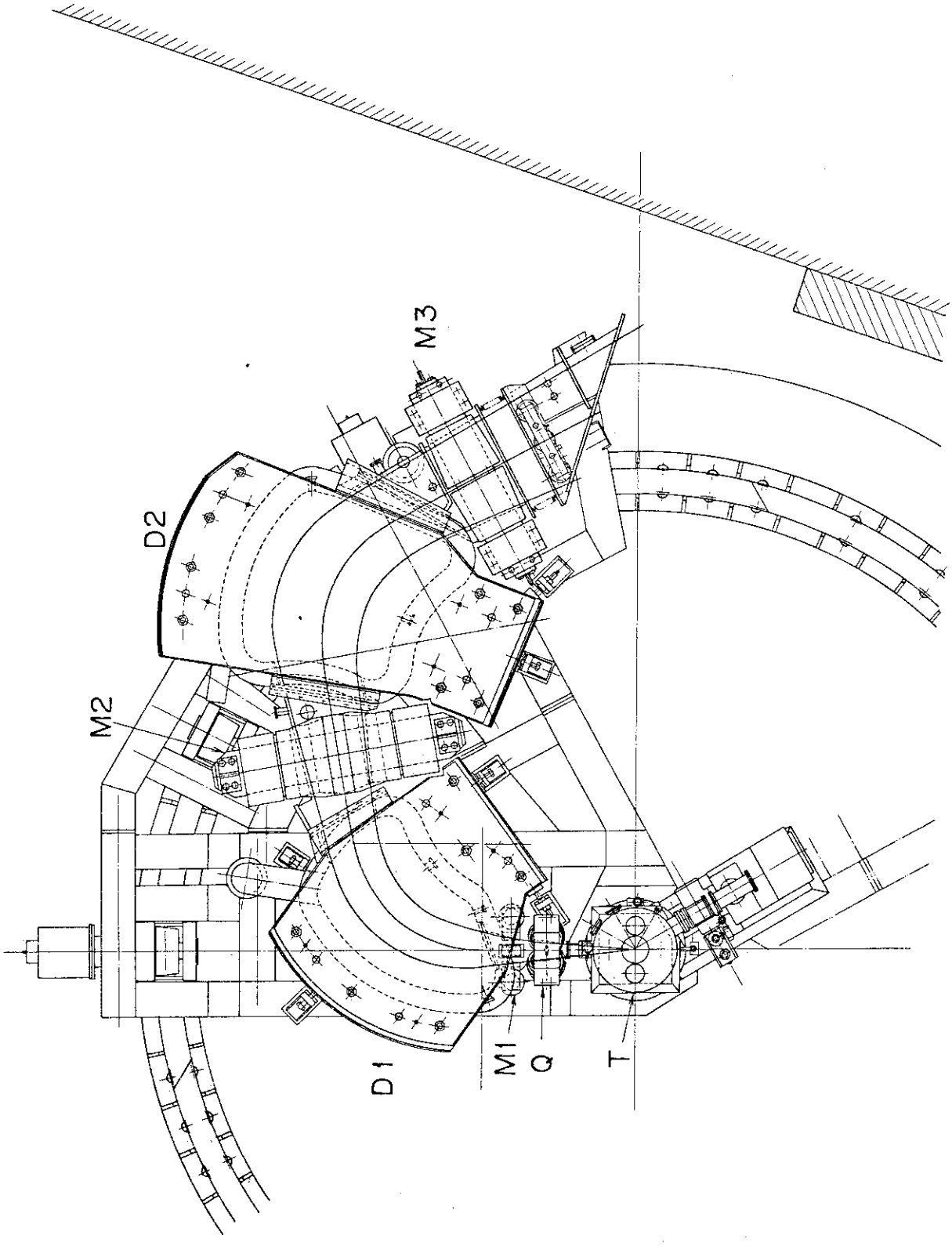

Fig.1 Geometrical arrangement of the spectrograph. T;target chamber, Q;quadrupole magnet, M1,M2,M3;multipole magnets, D1,D2;dipole magnets

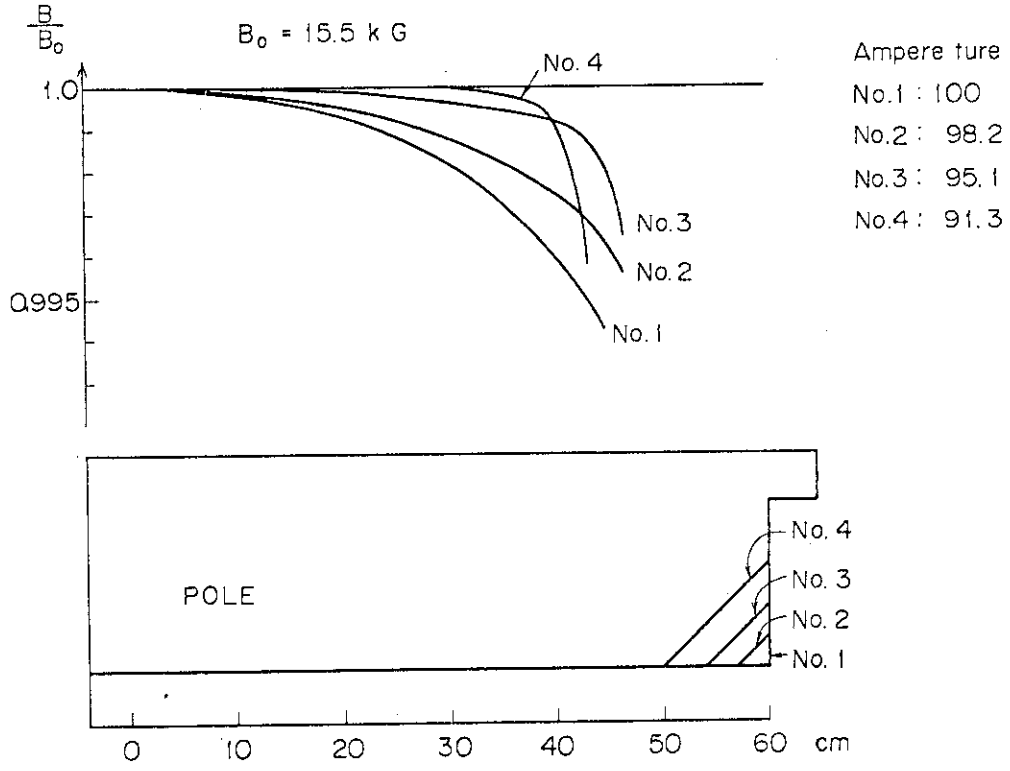

Fig.2 Calculated field distributions for different shapes of the pole edge. The relative values of the ampere-turns are also shown.

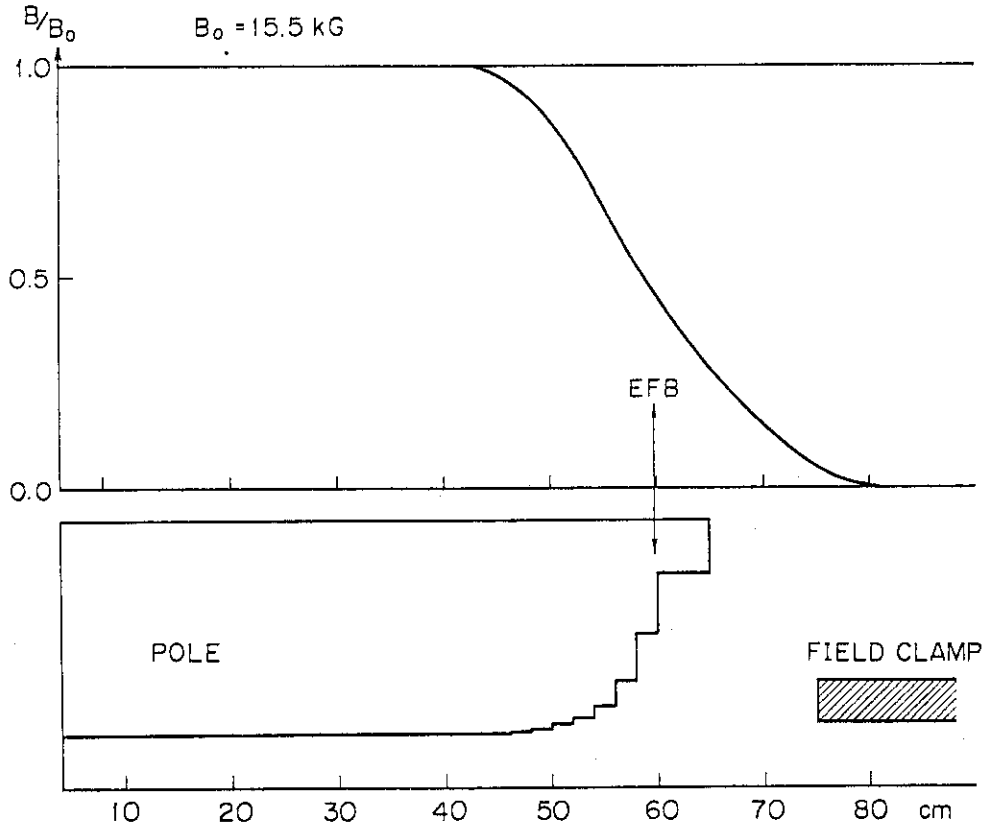

Fig.3 Adopted shape of the pole edge, the position of the field clamp, the calculated fringing field distribution and the effective field boundary (EFB) for the D2 magnet.

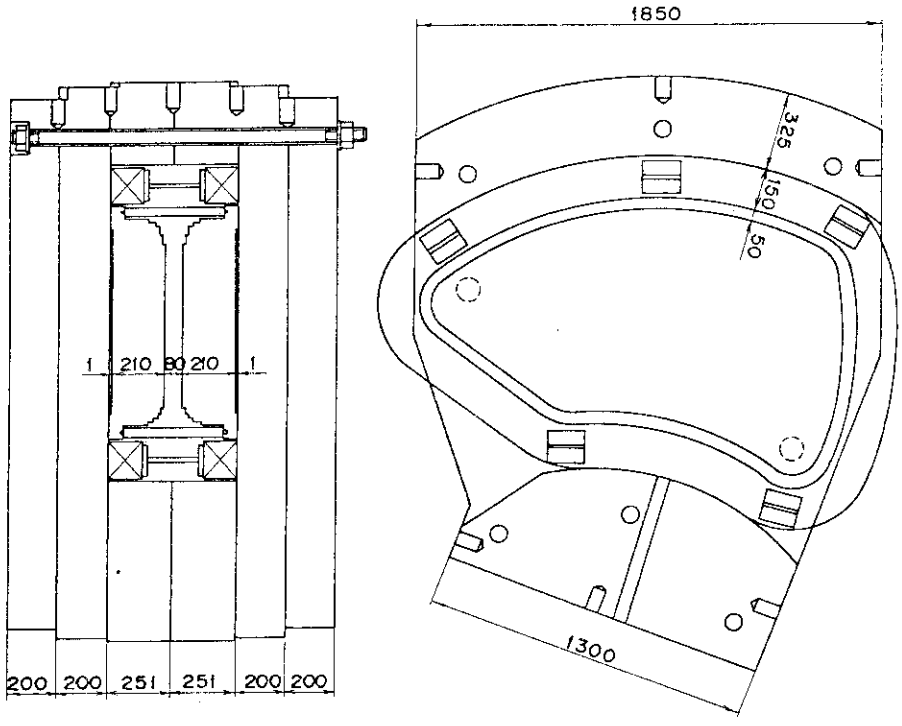

Fig.4 Cross-sectional view of the D1 magnet.

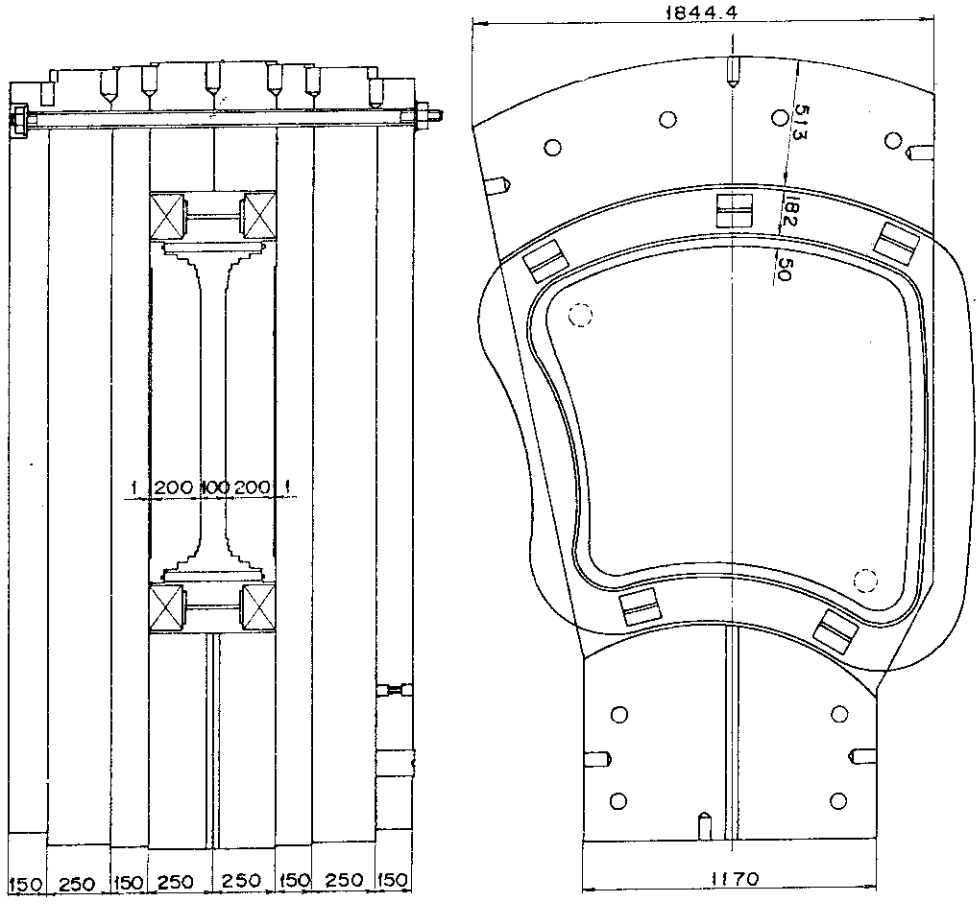

Fig.5 Cross-sectional view of the D2 magnet.

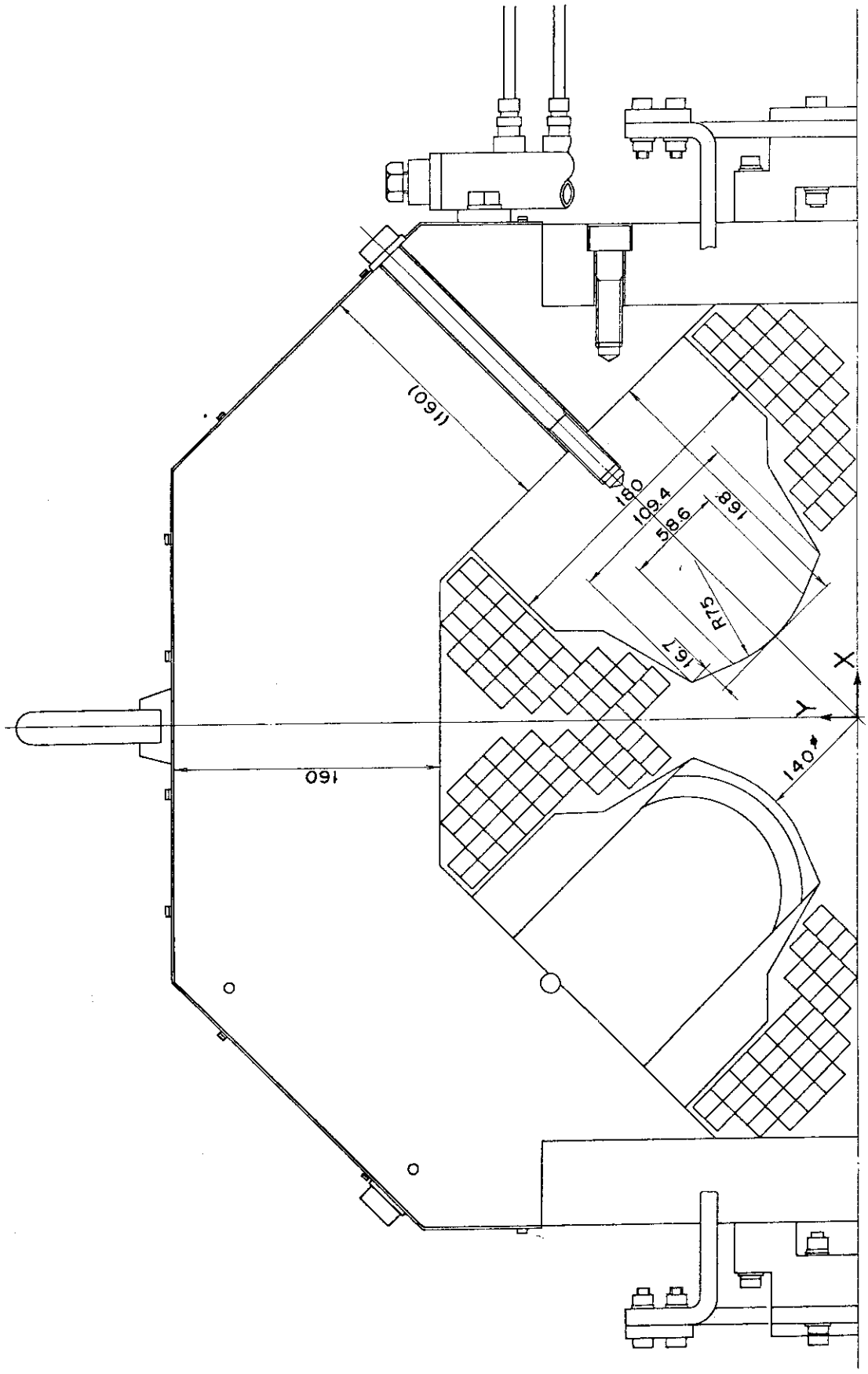

Fig.6 Cross-sectional view of the Q magnet.

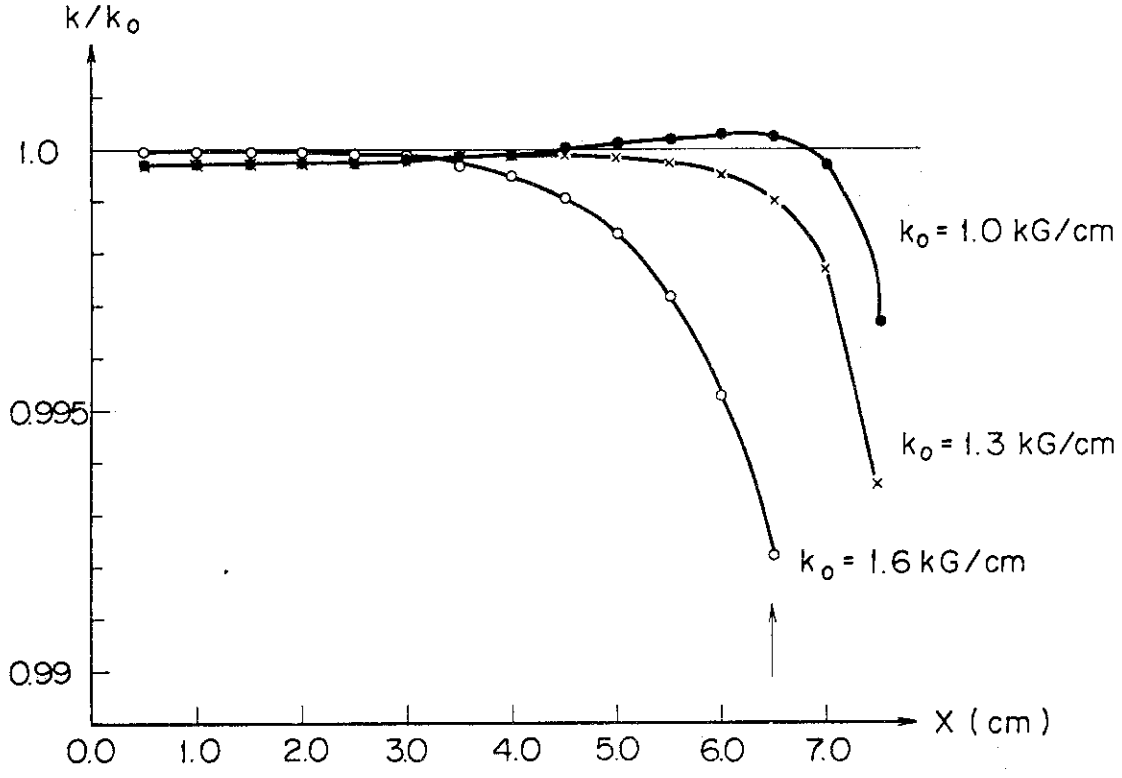

Fig.7 Calculated distributions of the field gradients k of the Q magnet for various field strength along the x-axis at the middle of the magnet. The required beam apperpure is indicated by an arrow.

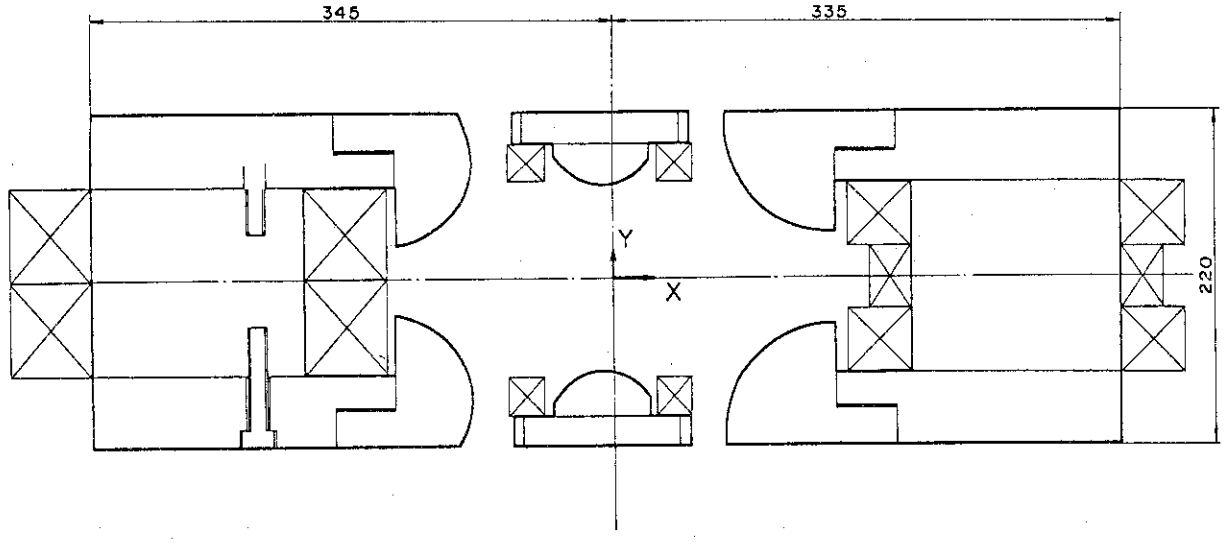

Fig.8 Cross-sectional view of the M1 magnet.

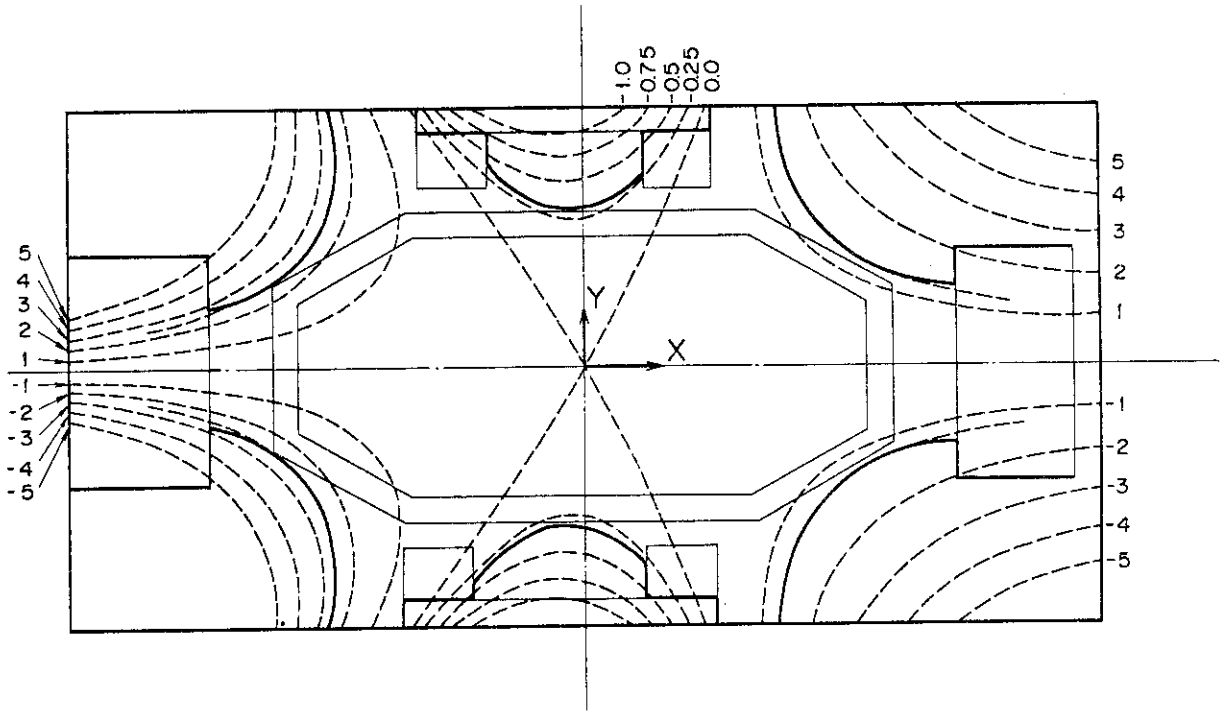

Fig.9 Magneto-static equi-potential contours (dotted line) and the pole configuration (solid line) of the M1 magnet. The vacuum chamber is also shown by solid lines. Figures indicate values of potential ϕ(M1) of eq. (2) divided by 10^3.

M 1

$$\Delta B = B_y - (k_6 x^2 + k_8 x^3)$$

$k_6 = 40$ G/cm^2

$k_8 = 1.28$ G/cm^3

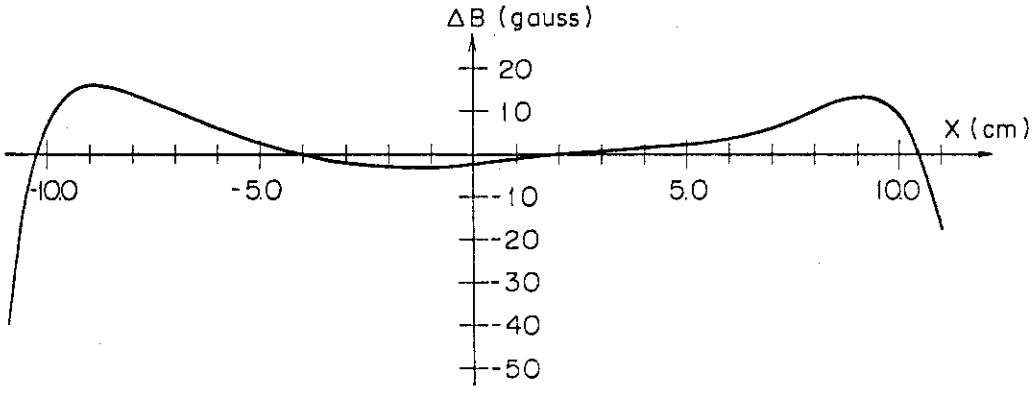

Fig.10 Calculated field distribution of the M1 magnet. The deviation of the field distribution from the ideal one is shown along the x-axis in the midplane.

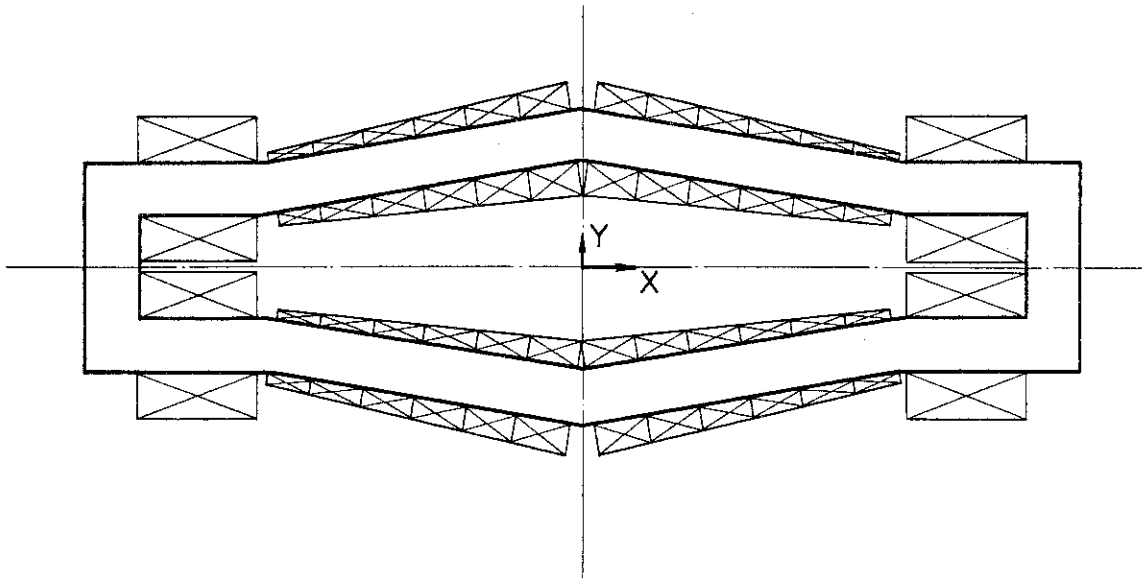

Fig.11 Schematical representation for the M2 and M3 magnets.

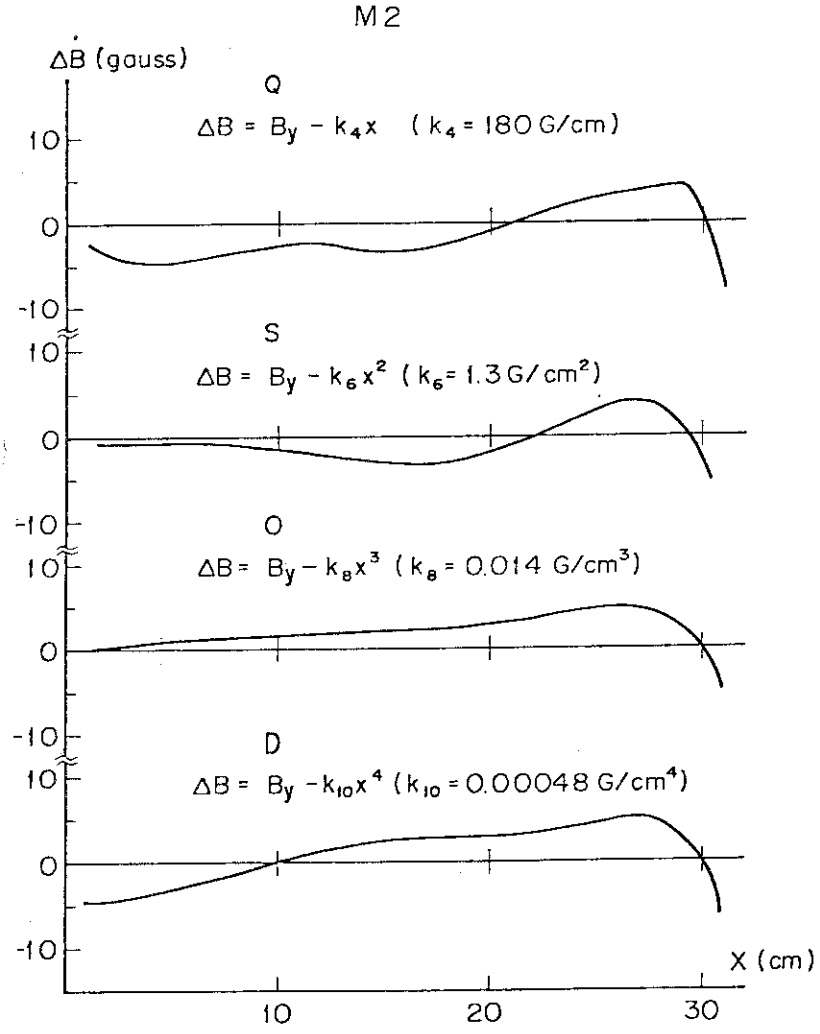

Fig.12 Calculated field distribution B_y of each multipole component of the M2 magnet. Deviations of each component from the ideal one are shown along the x-axis in the midplane. Q;quadrupole, S;sextupole, O;octupole, D;decapole

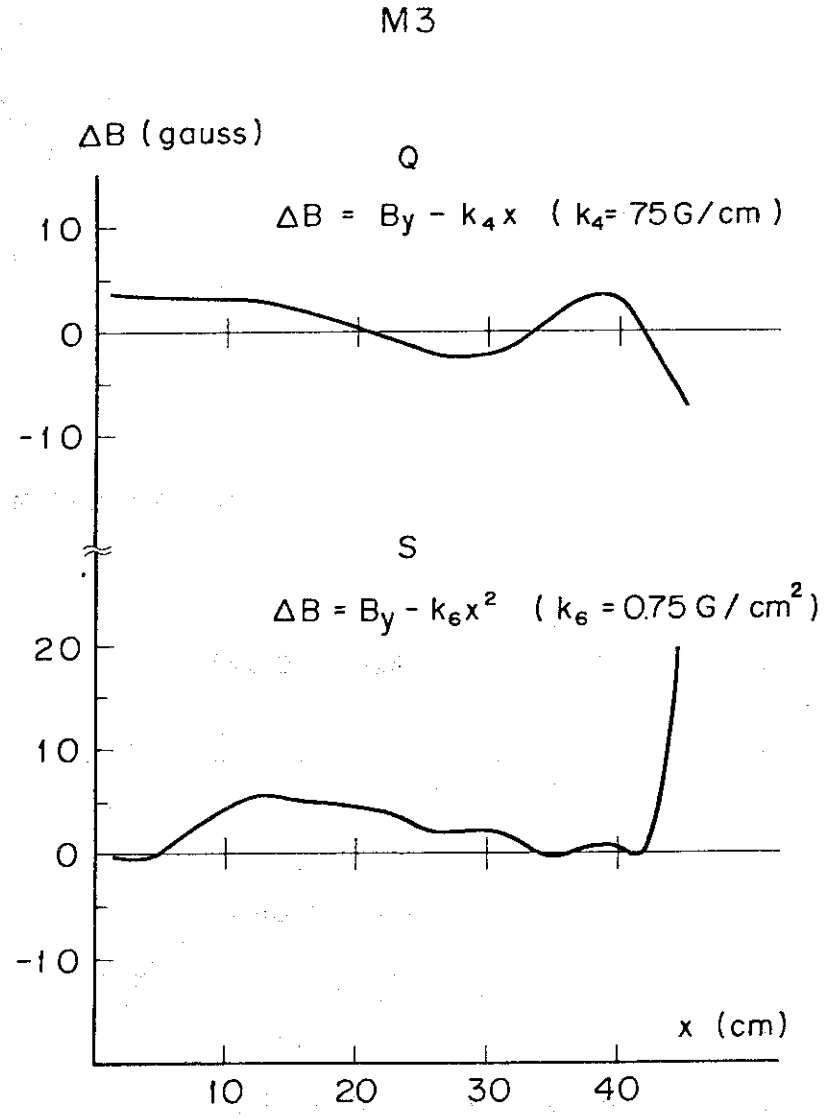

Fig.13 Calculated field distribution B_y of each multipole component of the M3 magnet. Deviations of each component from the ideal one are shown along the x-axis in the midplane for quadrupole (Q) and sextupole (S) components.